

Analytic vortex solutions on compact hyperbolic surfaces

Rafael Maldonado* and Nicholas S. Manton†

*Department of Applied Mathematics and Theoretical Physics,
Wilberforce Road, Cambridge CB3 0WA, U.K.*

August 27, 2018

Abstract

We construct, for the first time, Abelian-Higgs vortices on certain compact surfaces of constant negative curvature. Such surfaces are represented by a tessellation of the hyperbolic plane by regular polygons. The Higgs field is given implicitly in terms of Schwarz triangle functions and analytic solutions are available for certain highly symmetric configurations.

1 Introduction

Consider the Abelian-Higgs field theory on a background surface M with metric $ds^2 = \Omega(x, y) (dx^2 + dy^2)$. At critical coupling the static energy functional satisfies a Bogomolny bound

$$E = \frac{1}{2} \int \left(\frac{B^2}{2\Omega} + |D_i \Phi|^2 + \frac{\Omega}{2} (1 - |\Phi|^2)^2 \right) dx dy \geq \pi N, \quad (1)$$

where the topological invariant N (the ‘vortex number’) is the number of zeros of Φ counted with multiplicity [1]. In the notation of [2] we have taken $e^2 = \tau = 1$. Equality in (1) is attained when the fields satisfy the Bogomolny vortex equations, which are obtained by completing the square in (1). In complex coordinates $z = x + iy$ these are

$$D_{\bar{z}} \Phi = 0, \quad B = \Omega (1 - |\Phi|^2). \quad (2)$$

This set of equations has smooth vortex solutions. As we explain in section 2, analytical results are most readily obtained when M is hyperbolic, having constant negative curvature $K = -1$, a case which is of interest in its own right due to the relation between hyperbolic vortices and $\text{SO}(3)$ -invariant instantons, [3].

The aim of this paper is to construct solutions to the vortex equations on *compact* surfaces M whose universal cover has a hyperbolic metric. In section 3 we will see how such surfaces can be obtained as quotients of the hyperbolic plane. The problem of

*R.Maldonado@damtp.cam.ac.uk

†N.S.Manton@damtp.cam.ac.uk

finding one vortex on M is then equivalent to finding a regular lattice of vortices in the hyperbolic plane, which may be of interest as a hyperbolic version of the Abrikosov vortex lattice observed experimentally in superconductors [4].

Our approach involves the construction of the Higgs field Φ from a holomorphic function $f(z)$ satisfying certain periodicity conditions. The bulk of this paper (section 4) is concerned with constructing this map for an especially symmetric genus 2 surface, the Bolza surface. Section 5 extends the construction to certain higher genus surfaces and we wrap up in section 6 with some ideas for future work.

2 Hyperbolic vortices

The Bogomolny equations (2) for Abelian-Higgs vortices at critical coupling on a curved surface can be combined to give the Taubes equation

$$\nabla^2 \log |\Phi|^2 + 2\Omega(1 - |\Phi|^2) = 4\pi \sum_{i=1}^N \delta^{(2)}(z - z_i). \quad (3)$$

The right hand side provides sources for the vortices, where the Higgs field Φ vanishes. The Higgs field can be written as $\Phi = e^{h/2+i\chi}$ with h and χ real functions of z and \bar{z} . The phase χ depends on the gauge choice and increases by 2π around a unit charge vortex. Expressed in terms of these functions, the components of the 1-form gauge potential and magnetic flux density are

$$a_{\bar{z}} = a_z^* = -i\partial_{\bar{z}}\left(\frac{1}{2}h + i\chi\right), \quad B = -2iF_{z\bar{z}} = -2i(\partial_z a_{\bar{z}} - \partial_{\bar{z}} a_z) = -\frac{1}{2}\nabla^2 h, \quad (4)$$

where $\nabla^2 = 4\partial_z\partial_{\bar{z}}$ is the naive Euclidean Laplacian.

It was first observed by Witten, [3], that on a background of constant negative Gaussian curvature

$$K(z, \bar{z}) = -\frac{1}{2\Omega} \nabla^2 \log(\Omega) = -1, \quad (5)$$

the Taubes equation becomes the Liouville equation and can be solved exactly. We work with the Poincaré disk model of the hyperbolic plane, with metric

$$ds^2 = \frac{4}{(1 - |z|^2)^2} dzd\bar{z}. \quad (6)$$

Geodesics for this metric are circular arcs which intersect the boundary of the unit disk at right angles, and the geodesic distance between two points is

$$d(z_2, z_1) = \cosh^{-1} \left(1 + \frac{2|z_2 - z_1|^2}{(1 - |z_1|^2)(1 - |z_2|^2)} \right). \quad (7)$$

The general solution to the Taubes equation (3) constructed by Witten is a Higgs field

$$\Phi(z, \bar{z}) = \frac{1 - |z|^2}{1 - |f(z)|^2} \frac{df}{dz}, \quad (8)$$

so $|\Phi|^2$ is a ratio of two hyperbolic metrics of equal curvature [2],

$$|\Phi|^2 = \frac{\tilde{\Omega}(f(z))}{\Omega(z)} \left| \frac{df}{dz} \right|^2. \quad (9)$$

The function $w = f(z)$ is holomorphic with $|f| < 1$ on the interior of the disk and $|f| = 1$ on the boundary $|z| = 1$, so $f : z \rightarrow w$ is a map from the Poincaré disk to itself. The map has ramification points at the vortex positions, where, for a vortex of unit multiplicity, Φ has a simple zero and $f(z)$ behaves locally quadratically. Solving the Taubes equation on hyperbolic space thus boils down to finding a holomorphic map $f : \mathbb{H}^2 \rightarrow \mathbb{H}^2$ with ramification points of order one greater than the multiplicity of Φ at each vortex position. The Schwarz-Pick lemma guarantees that $|\Phi| < 1$ on the interior of the disk, with $|\Phi| = 1$ everywhere on the boundary (where the Higgs field takes its vacuum value).

Let us consider the case where the domain of f is a compact surface (M, Ω) of area A_M and genus g . Then the target surface $(\tilde{M}, \tilde{\Omega})$ has a finite area which is obtained by pulling back the area form on \tilde{M} by f . Integrating the Taubes equation (3) over M and using the topological invariant $\int B dx dy = 2\pi N$ gives

$$A_{\tilde{M}} = \int_{\tilde{M}} dA_{\tilde{M}} = \int_M |\Phi|^2 \Omega dx dy = \int_M \Omega dx dy - 2\pi N = A_M - 2\pi N, \quad (10)$$

where N is the number of zeros of Φ counted with multiplicity. Positivity of $A_{\tilde{M}}$ implies the Bradlow bound on the number of vortices on a compact surface:

$$2\pi N < A_M = 4\pi(g - 1), \quad (11)$$

where the relation between the area and genus of the surface M follows from the Gauss-Bonnet theorem $\int(-K)dA = 4\pi(g - 1)$. The vacuum solution with $N = 0$ has $\Phi = 1$ everywhere, while at the Bradlow limit $\Phi = 0$. The interpretation is that each vortex takes up an effective area 2π .¹

It is important to check that there is no contribution from the cross term arising when completing the square in (1). This term is a total derivative and vanishes identically on a compact surface.

Multivaluedness of f means that the area of each sheet of \tilde{M} is in fact the value of $A_{\tilde{M}}$ given in (10) divided by one plus the number of vortices on the interior of M . This is in essence the Riemann-Hurwitz theorem and will be important in sections 4 and 5, where \tilde{M} is considered as a tessellation of \mathbb{H}^2 .

¹The Bradlow bound (11) can be modified to allow for an arbitrary number of vortices on the surface. By changing the potential term in (1) to $\Omega(\tau - |\Phi|^2)^2/2$, the Bradlow inequality becomes $2\pi N < \tau A_M$. However, this has the effect of changing the curvature of the target space to $K_{\tilde{M}} = -\tau$, and the Taubes equation is no longer integrable.

Example I: a finite number of vortices

For a finite number of vortices, N , on \mathbb{H}^2 , the function $f(z)$ is a Blaschke product [3]

$$f(z) = \prod_{j=1}^{N+1} \frac{z - a_j}{1 - \bar{a}_j z}, \quad |a_j| < 1 \quad \forall j. \quad (12)$$

In general the relation between the complex numbers a_j and the vortex positions (at the critical points of f) is not obvious. Constructing a vortex solution from the vortex positions can only be done analytically for symmetric configurations, such as a cyclic ring of vortices. The parameters needed for an arbitrary prescribed vortex arrangement must be found numerically.

Example II: a singly periodic array

A vortex solution on the hyperbolic cylinder \mathbb{H}^2/\mathbb{Z} was presented in [5]. The solution was constructed via a map f from a half annulus in the upper half plane to a Euclidean rectangle, giving rise to a doubly periodic function. In Poincaré disk coordinates, f is given by a ratio of Jacobi elliptic functions,

$$f(z) = \frac{\text{cd}\left(\frac{4\mathbf{K}}{\pi} \tan^{-1}(z); k\right) - 1}{\text{cd}\left(\frac{4\mathbf{K}}{\pi} \tan^{-1}(z); k\right) + 1}. \quad (13)$$

Vortices (i.e. zeros of $f'(z)$) are located at $z = i \tanh(n\lambda/4)$ with $\lambda = \pi\mathbf{K}'/\mathbf{K}$ and $n \in \mathbb{Z}$, where $\mathbf{K}(k)$ is the complete elliptic integral of the first kind with elliptic modulus k , and $\mathbf{K}'(k) = \mathbf{K}(\sqrt{1-k^2})$. Notice that there is a double zero of $f(z)$ at every other zero of Φ . This suggests that f can be expressed as an infinite Blaschke product

$$f(z) = z^2 \prod_{j=1}^{\infty} \left(\frac{z^2 - a_j^2}{1 - a_j^2 z^2} \right)^2 \quad \text{with} \quad a_j = i \tanh\left(\frac{j\lambda}{2}\right). \quad (14)$$

Equality between (13) and (14) is easily checked at $z = i \tanh(n\lambda/4)$ by known infinite products. The *Blaschke condition*

$$\sum_{j=1}^{\infty} (1 - |a_j|) < \infty \quad (15)$$

holds for $\lambda > 0$ (the sum can be evaluated as a q -hypergeometric function), thereby ensuring convergence of the product (14).

Using the closed form expression (13), the Higgs field (8) near the vortex at the origin and at the midpoint between vortices is

$$|\Phi|_{\text{origin}} = \frac{8\mathbf{K}^2}{\pi^2} (1 - k^2) |z| + \dots, \quad |\Phi|_{\text{midpoint}} = \frac{2\mathbf{K}}{\pi} (1 - k). \quad (16)$$

Periodicity of $|\Phi|$ follows from the fact that a period shift in z is equivalent to a fractional linear transformation of f :

$$z \mapsto z' = \frac{z - i \tanh(\lambda/4)}{iz \tanh(\lambda/4) + 1} \quad \Rightarrow \quad f(z') = \frac{(1+k)f(z) - (1-k)}{(1-k)f(z) - (1+k)}, \quad (17)$$

a symmetry which will be discussed in more detail in section 4.1.

3 Hyperbolic tessellations

The hyperbolic plane has infinitely many tessellations by regular polygons whose edges are geodesic arcs. Such tessellations are denoted by their Schläfli symbol $\{p, q\}$, where p is the number of sides of the fundamental polygon and q the number of such polygons meeting at each vertex. These polygons tile the hyperbolic plane if $q(p-2) > 2p$ and, in contrast to the case of tessellations of the Euclidean plane, have a fixed area

$$A_{\{p,q\}} = \frac{\pi}{(-K)} \left(p - 2 - \frac{2p}{q} \right), \quad (18)$$

where in our conventions $K = -1$.

We follow [6] in defining the Euler characteristic of any regular tessellation to be

$$\chi_{\{p,q\}} = -A_{\{p,q\}}/2\pi. \quad (19)$$

As discussed below, a given tessellation describes a smooth compact surface of genus g if χ is a negative even integer, $\chi = 2 - 2g$. The surface is obtained by identifying pairs of edges of the fundamental polygon.

The uniformization theorem guarantees that a compact surface M of genus $g \geq 2$ possesses a global hyperbolic metric. The universal covering space of such a surface is the hyperbolic plane, with a tessellation whose fundamental domain is obtained as the quotient \mathbb{H}^2/H , where $H \cong \pi_1(M)$ is the first homotopy group of the surface. The usual application of the Gauss-Bonnet theorem tells us that the area of a compact genus g surface with curvature $K = -1$ is $A = -2\pi\chi = 4\pi(g-1)$. Note from (18) that a tessellation with $\{p, q\} = \{4g, 4g\}$ has the correct area for a surface of genus g .

For given g , there is a $3(g-1)$ -complex-dimensional family of surfaces parametrised by the lengths of $3(g-1)$ non-intersecting closed geodesics on the fundamental polygon, together with ‘twist’ data describing the gluing of the edges. These parameters are known as the Fenchel-Nielsen coordinates on Teichmüller space, [7]. For ease of computation we specialise to the most symmetric surfaces, corresponding to tessellations by regular polygons. As an example, a smooth genus 2 surface can be constructed from any of the tessellations

$$\{8, 8\}, \quad \{10, 5\}, \quad \{12, 4\}, \quad \{18, 3\}.$$

Of the tessellations above, our focus will be mainly on the highly symmetric tessellation by regular octagons in the $\{8, 8\}$ configuration with opposite edges identified. Such a

tessellation is obtained as the quotient of the unit disk by the freely acting subgroup $H \subset \Gamma$ of the full automorphism group Γ of the tessellation. H is a Fuchsian group generated by eight hyperbolic Möbius transformations M_k . This is a discrete subgroup of $\text{PSL}(2, \mathbb{C})$ with the fixed-point-free condition $(\text{tr} M_k)^2 > 4$. Note that Γ also contains elliptic elements with fixed points in the interior of the disk; these elements are excluded from the quotient in order to obtain a smooth surface. If we orient the tessellation such that there are octagon centres at the origin and along the coordinate axes, then the eight Möbius transformations $M_k(z)$ with $k = 0, \dots, 7$ take the form

$$M_k(z) = \frac{z + Le^{ik\pi/4}}{Le^{-ik\pi/4}z + 1} \quad \text{with} \quad L = \sqrt{2\sqrt{2} - 2} \approx 0.910, \quad (20)$$

where L is the Euclidean distance from the origin to one of the neighbouring octagon centres and we have the relation $M_{k+4} = M_k^{-1}$. This identification of the tessellation amounts to defining the fundamental octagon, \mathcal{O} , by

$$\mathcal{O} = \{x \in \mathbb{H}^2 \mid d(x, 0) \leq d(x, M_k(0)), k = 0, \dots, 7\}, \quad (21)$$

where the hyperbolic distance function was defined in (7). Note that hyperbolic tessellations do not, in general, correspond to compact surfaces, but a fundamental polygon can still be defined as in (21), and the tessellation has a fractional Euler characteristic defined by (19).

The fundamental polygon of the regular $\{8, 8\}$ tessellation with opposite edges identified is the most symmetric genus 2 surface, known as the Bolza surface. It has an automorphism group of order 48 (96 if one includes reflections) and can be thought of as a double cover of \mathbb{CP}^1 with ramification points at the six vertices of an inscribed regular octahedron. On the hyperbolic octagon, the ramification points correspond to points of C_8 symmetry. There are also 16 points with C_3 symmetry and 24 with C_2 symmetry, as can be seen by dividing the octagon into 96 triangles with angles $(\frac{\pi}{2}, \frac{\pi}{3}, \frac{\pi}{8})$. Most of this symmetry is broken when a vortex is placed on the surface. However, when the vortex is placed at the origin, the C_8 symmetry about both the origin and the vertex is preserved, which will be key to our analytical construction. The fundamental domain for the $\{8, 8\}$ tessellation, together with the positions of the symmetric points, is sketched in figure 1. As a hyperelliptic curve, the genus 2 Bolza surface can be expressed as

$$y^2 = x(x^4 + 1). \quad (22)$$

We will return to the representation of the Bolza surface as a hyperelliptic curve in the context of compact surfaces of higher genus in section 5.

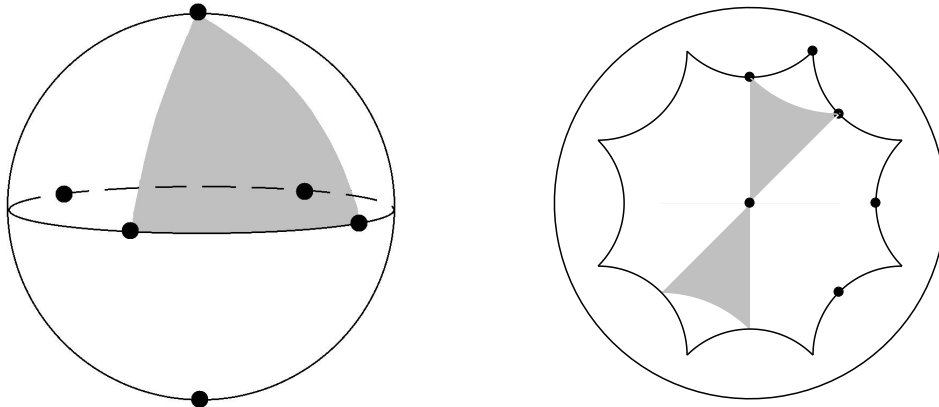


Figure 1: The Bolza surface can be represented as a double cover of the Riemann sphere branched at the vertices of an inscribed regular octahedron (left), or equivalently as an $\{8, 8\}$ tessellation of the hyperbolic plane (right) where opposite edges of the fundamental octagon are identified. There is a C_8 symmetry at each of the branch points, which are indicated by dots. The shaded equilateral triangle with angles $\pi/2$ on the sphere is covered by the two shaded equilateral triangles with angles $\pi/4$ on the Bolza surface (one for each branch). The north and south poles of the sphere correspond to the centre and vertex of the octagon, and hence to antipodal points on the Bolza surface.

4 A vortex on the Bolza surface

4.1 Identifying the holomorphic map

The aim of this section is to compute the Higgs field of a vortex placed at the centre of the period octagon. As described in section 2, we proceed by looking for a holomorphic function $f : \mathbb{H}^2 \rightarrow \mathbb{H}^2$ ramified at the centre of every octagonal cell in the tessellation. Restricted to the fundamental octagon, the map $w = f(z)$ is conformal except at the vortex position, where angles are doubled. The image is precisely a square in the $\{4, 8\}$ tessellation, and the map f is two-to-one, providing a double cover of the square with double winding around the centre. Pairs of identified opposite edges of the octagon map to the same edge of the square. It should be noted that opposite edges of the square are not identified, as the $\{4, 8\}$ tessellation does not correspond to a compact surface. A Möbius transformation (20) mapping one vortex to the next corresponds to a rotation about one of the four edge centres of the fundamental square,

$$\tilde{M}_k(f(z)) = f(M_k(z)) = \frac{\sqrt{2}f(z) - Le^{ik\pi/2}}{Le^{-ik\pi/2}f(z) - \sqrt{2}}, \quad (23)$$

which we deduce by considering the effect of f on the vertices of the octagon.

The fact that f transforms by a Möbius transformation shows that it is *not*, as might have been expected, an automorphic form. Instead, if z and $f(z)$ both transform

by fractional linear transformations

$$z \mapsto \frac{bz + c}{\bar{c}z + \bar{b}}, \quad f(z) \mapsto \frac{\beta f(z) + \gamma}{\bar{\gamma} f(z) + \bar{\beta}}, \quad (24)$$

with $|b|^2 - |c|^2 = 1 = |\beta|^2 - |\gamma|^2$, then $\frac{df}{dz}$ transforms as

$$\frac{df}{dz} \mapsto \left(\frac{\bar{c}z + \bar{b}}{\bar{\gamma} f(z) + \bar{\beta}} \right)^2 \frac{df}{dz}. \quad (25)$$

For the specific case in question, with the fractional linear transformations (20) and (23), we have

$$\frac{df}{dz} \mapsto (2\sqrt{2} + 4) \left(\frac{Le^{-ik\pi/4}z + 1}{Le^{-ik\pi/2}f(z) - \sqrt{2}} \right)^2 \frac{df}{dz}. \quad (26)$$

The factor multiplying $\frac{df}{dz}$ can be thought of as a gauge transformation of the vortex fields, which does not affect $|\Phi|$. Despite this complicated transformation property of f and $\frac{df}{dz}$, we will see in section 4.2 that automorphic forms do in fact appear in our computation of the vortex fields.

The area of the image square follows from the Riemann-Hurwitz theorem. Denote by A and A' the areas of the fundamental polygons in the domain and image tessellations, which are related to the Euler characteristic of the tessellation via (19). The map f has a single ramification point of order 2, so $A' = \frac{1}{2}(A - 2\pi)$ in agreement with (18), which gives $A_{\{8,8\}} = 4\pi$ and $A'_{\{4,8\}} = \pi$. More generally, if N vortices are placed in the interior of a domain polygon representing a compact genus g surface, then the map f has N ramification points and is of degree $N + 1$. By the Riemann-Hurwitz theorem, the area of the image polygon is given by

$$A' = \frac{1}{N + 1} (A - 2\pi N) = \frac{2\pi}{N + 1} (2g - 2 - N). \quad (27)$$

The requirement that $A' > 0$ implies that the number of vortices permitted on a genus g surface is constrained by

$$N < 2g - 2, \quad (28)$$

the Bradlow bound (11) again. The map we have described between the octagon and the square can hence be generalised to more vortices on a higher genus surface (see also sections 4.3 and 5).

Non-existence of Blaschke product

Before proceeding any further, we should investigate whether the map f can be expressed as an infinite Blaschke product with zeros of f occurring at the same density as vortices, mimicking the way this was done for the one-dimensional vortex array (13, 14). For f of the form (12) with $N \rightarrow \infty$, this will be the case if the Blaschke condition (15) holds.

Consider a circle $|z| = r$ in the Poincaré disk with $0 \ll r < 1$. As each octagon in the tessellation has area 4π , the interior of the circle will contain $N(r) = A(r)/4\pi =$

$r^2/(1-r^2)$ vortices. Then the number of vortices in an annulus of thickness dr is $dN = 2rdr/(1-r^2)^2$. Using this measure, the sum (15) can be converted to an integral if we assume that the $\{|a_j|\}$ have the density of the tessellation:

$$\sum_{j=1}^{\infty} (1 - |a_j|) \sim \lim_{\epsilon \rightarrow 0} \int^{1-\epsilon} (1-r) \frac{2r}{(1-r^2)^2} dr. \quad (29)$$

The right hand side diverges logarithmically, hence there is no convergent Blaschke product with the symmetries of the octagonal tessellation. For the hyperbolic cylinder discussed in section 2 the number of vortices as a function of distance from the origin is $N(r) \propto \tanh^{-1} r$, so $dN \propto dr/(1-r^2)$ and the corresponding integral converges.

4.2 Mapping between polygons

The map f between the polygonal tessellations of the Poincaré disk described in section 4.1 is easy to implement because the position of the vortex is consistent with a regular tiling of the fundamental polygon by congruent triangles with a shared vertex at the vortex position. This procedure avoids mapping directly between the octagon and the square, which would introduce a large number of additional *accessory parameters* which would then need to be determined. We thus divide the fundamental octagon into 16 triangles, each of which maps, via an auxiliary half plane, to an eighth of the image square. The fundamental domains \mathcal{O}_Δ (with Poincaré disk coordinate z) and \mathcal{S}_Δ (with coordinate w) are shown in figure 2. By Schwarz reflection, the hyperbolic plane is covered by repeated reflection of the triangle \mathcal{O}_Δ in its edges.

The existence of the maps in figure 2 is guaranteed by the Riemann mapping theorem. In the following paragraphs we sketch how the Riemann map is constructed for curvilinear polygons before specialising to the case of triangles, where one can obtain explicit results. Then in section 4.3 we will focus on the specific triangles in figure 2.

The Riemann map

The Riemann mapping theorem states the existence of a unique conformal map between the upper half plane and the interior of a simply connected domain of \mathbb{C} . Specialising to the case of an n -sided polygon bounded by circular arcs, the map is bijective and extends to a map from the boundary of the upper half plane to the boundary of the polygon. It is conformal everywhere except at the n points ζ_i on the real axis which map to the vertices of the polygon. The requirement that the image of the map should extend to the entire Poincaré disk by a series of reflections leads to an $\text{SL}(2, \mathbb{R})$ -invariant differential equation satisfied by the function s representing the map. This third order non-linear ordinary differential equation is solved by a ratio of linearly independent solutions to a second order linear ordinary differential equation with n regular singular points at $\zeta = \zeta_i$, where the exponents depend on the angle at each corresponding vertex of the polygon. The interested reader is referred to [8] for details. From now on we specialise to the case of triangles, in which case the Riemann map is known as the Schwarz triangle map.

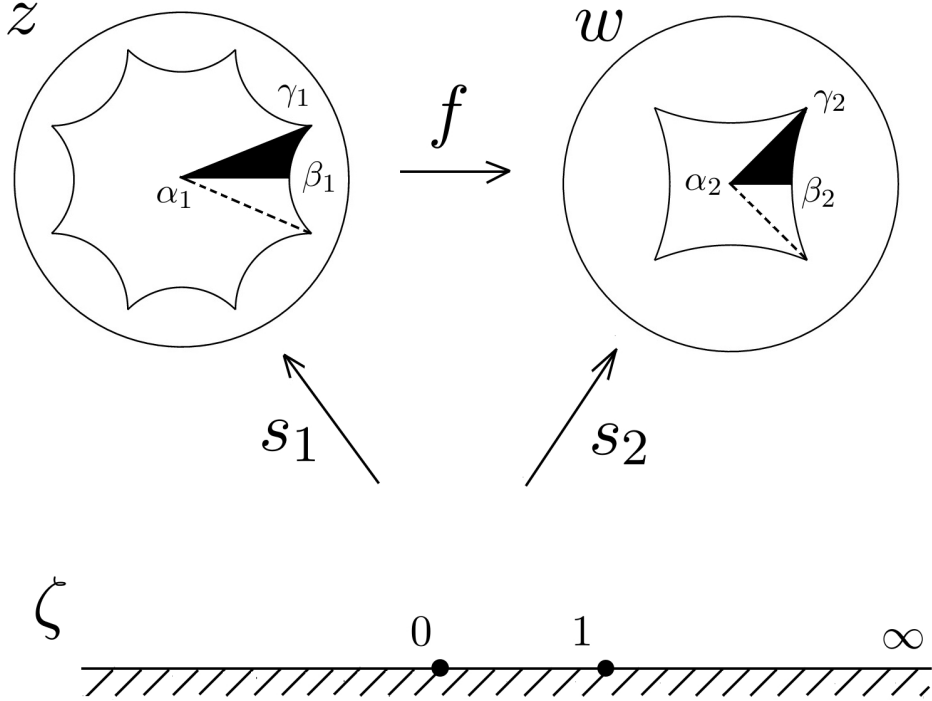


Figure 2: Sketch showing the action of the map f on a triangle \mathcal{O}_Δ within the fundamental octagon \mathcal{O} , via an auxiliary upper half plane. The image square and triangle are denoted \mathcal{S} and \mathcal{S}_Δ . In our conventions, $\zeta = 0$ maps to the vertex of the shaded triangles at the origin of the tessellations, while $\zeta = 1$ and $\zeta = \infty$ map to the other two vertices, respectively the edge midpoint and vertex of the polygons. The real axis of the upper half plane maps to the boundary of the triangle. The angles of the black triangles are $(\pi\alpha_1, \pi\beta_1, \pi\gamma_1) = (\frac{\pi}{8}, \frac{\pi}{2}, \frac{\pi}{8})$ and $(\pi\alpha_2, \pi\beta_2, \pi\gamma_2) = (\frac{\pi}{4}, \frac{\pi}{2}, \frac{\pi}{8})$. The Higgs field at a vertex of the octagon is easier to compute if we instead use the dashed triangles, which has the effect of swapping β and γ .

The Schwarz triangle map

In order to make use of the Riemann mapping theorem we introduce an auxiliary upper half plane with complex coordinate ζ . Then there are two Schwarz triangle maps, $s_1 : \zeta \rightarrow z$ and $s_2 : \zeta \rightarrow w$, mapping the upper half plane to each of the triangles in figure 2. The map f between the triangles \mathcal{O}_Δ and \mathcal{S}_Δ is given by the composition $w = f(z) = s_2(s_1^{-1}(z))$. Note that when the images are extended to the entirety of the Poincaré disk (by reflections both in the triangle edges and from the auxiliary upper half plane to the lower half plane), the functions $s_1(\zeta)$ and $s_2(\zeta)$ are multivalued. On the other hand, the inverse maps $s_1^{-1}(z)$ and $s_2^{-1}(w)$ are automorphic forms invariant under the elements of the automorphism group of the octagon, and are dense in both zeros and poles as the boundary of the disk is approached. In general there is no closed form expression for $s_1^{-1}(z)$, so we use a parametric approach: picking an arbitrary point on the ζ plane will tell us the value of $f(z)$ at $z = s_1(\zeta)$. As we shall see, there are some particular points on \mathcal{O}_Δ at which we can expand $f(z)$ as a series, allowing $\Phi(z)$ to be computed analytically using (8).

By convention, we take the points $\zeta_i = 0, 1, \infty$ on the upper half plane to map to the vertices of a triangle with angles $\pi\alpha, \pi\beta, \pi\gamma$, respectively. The map from the upper half plane to this triangle is given by a ratio of two linearly independent solutions of the hypergeometric equation [8]

$$\frac{d^2y}{d\zeta^2} + \left(\frac{c}{\zeta} + \frac{d}{\zeta-1} \right) \frac{dy}{d\zeta} + \frac{ab}{\zeta(\zeta-1)} y = 0. \quad (30)$$

The two solutions at $\zeta = 0$ have exponents 0 and $(1-c)$, and are given by the hypergeometric functions

$$y(\zeta) = F(a, b; c; \zeta) \quad \tilde{y}(\zeta) = \zeta^{1-c} F(a', b'; c'; \zeta), \quad (31)$$

where a, b, c and d are related to the angles of the triangle by

$$\left\{ \begin{array}{ll} a = \frac{1}{2}(1 - \alpha - \beta + \gamma) & a' = a - c + 1 \\ b = \frac{1}{2}(1 - \alpha - \beta - \gamma) & b' = b - c + 1 \\ c = 1 - \alpha & c' = 2 - c \\ d = 1 - \beta = a + b - c + 1 & d' = d. \end{array} \right. \quad (32)$$

The Schwarz triangle function is then defined as

$$s(\zeta) = \mathcal{N} \frac{\tilde{y}(\zeta)}{y(\zeta)}, \quad (33)$$

where the normalisation factor \mathcal{N} is chosen so as to ensure that the triangle has the correct size, such that geodesic extensions of the circular edges intersect the unit disk at right angles. This calculation was performed in [9]. Putting everything together and simplifying, we have

$$s(\zeta) = \sqrt{\frac{\sin(\pi a') \sin(\pi b')}{\sin(\pi a) \sin(\pi b)}} \frac{\Gamma(a') \Gamma(b') \Gamma(c)}{\Gamma(a) \Gamma(b) \Gamma(c')} \zeta^{1-c} \frac{F(a', b'; c'; \zeta)}{F(a, b; c; \zeta)}. \quad (34)$$

4.3 Computing the Higgs field

In order to calculate the Higgs field, we use the two triangle maps $s_1(\zeta)$ and $s_2(\zeta)$ as depicted in figure 2. The derivative of f is obtained by the chain rule. Then substituting into (8) gives

$$\Phi(z) = \frac{1 - |s_1(\zeta)|^2}{1 - |s_2(\zeta)|^2} \frac{ds_2(\zeta)}{d\zeta} \left(\frac{ds_1(\zeta)}{d\zeta} \right)^{-1}. \quad (35)$$

Recall that (α, β, γ) are the angles in the triangle (divided by π), and (a, b, c) are defined through (32). The triangles of interest (figure 2) have $(\alpha_1, \beta_1, \gamma_1) = (\frac{1}{8}, \frac{1}{2}, \frac{1}{8})$ and $(\alpha_2, \beta_2, \gamma_2) = (\frac{1}{4}, \frac{1}{2}, \frac{1}{8})$. The Higgs field of a vortex placed at the origin can be computed analytically at the vertices of the fundamental triangle \mathcal{O}_Δ . In order to do this, we expand $s(\zeta)$ near the singular points:

$$s(\delta) = \sqrt{\frac{\sin(\pi a') \sin(\pi b')}{\sin(\pi a) \sin(\pi b)}} \frac{\Gamma(a') \Gamma(b') \Gamma(c)}{\Gamma(a) \Gamma(b) \Gamma(c')} \delta^\alpha + \dots \quad (36)$$

$$s(1 + \delta) = \sqrt{\frac{\sin(\pi a) \sin(\pi b)}{\sin(\pi a') \sin(\pi b')}} \left(1 - \delta^\beta \frac{\sin(\pi \alpha)}{\pi \beta \Gamma^2(\beta)} \Gamma(1 - a) \Gamma(1 - b) \Gamma(1 - a') \Gamma(1 - b') + \dots \right) \quad (37)$$

The formula (35) then gives the Higgs field at the points on the octagon corresponding to the vertices of \mathcal{O}_Δ . Near $\zeta = 0$ we have from (36)

$$z = s_1(\zeta) = \mathcal{N}_1 \zeta^{1/8} + \dots, \quad s_2(\zeta) = \mathcal{N}_2 \zeta^{1/4} + \dots \quad (38)$$

Using (35) and the expansion of $s_1(\zeta)$ to change from ζ to z coordinates gives

$$\Phi = 2 \frac{\mathcal{N}_2}{\mathcal{N}_1} \zeta^{1/8} + \dots = 2 \frac{\mathcal{N}_2}{\mathcal{N}_1^2} z + \dots \quad (39)$$

At the vertex of \mathcal{O}_Δ corresponding to $\zeta = 1$, the expansion is of the form

$$s_1(1 + \delta) = \mathcal{A}_1 + \mathcal{B}_1 \delta^{1/2} + \dots, \quad s_2(1 + \delta) = \mathcal{A}_2 + \mathcal{B}_2 \delta^{1/2} + \dots, \quad (40)$$

with coefficients that can read off from (37). Applying (35) gives

$$\Phi = \frac{1 - \mathcal{A}_1^2}{1 - \mathcal{A}_2^2} \frac{\mathcal{B}_2}{\mathcal{B}_1}. \quad (41)$$

Evaluating (39) and (41) for the triangles of interest, we find

$$|\Phi|_{\text{origin}} = \left[(4\pi)^{-3/2} \sin\left(\frac{\pi}{8}\right) \Gamma^2\left(\frac{1}{8}\right) \Gamma\left(\frac{1}{4}\right) \right] |z| + \mathcal{O}(|z|^3) \approx 1.768|z| + \mathcal{O}(|z|^3), \quad (42)$$

$$|\Phi|_{\text{mid edge}} = \frac{\sqrt{2} \Gamma\left(\frac{1}{8}\right) \Gamma^2\left(\frac{1}{4}\right) \Gamma\left(\frac{3}{8}\right)}{\Gamma\left(\frac{1}{16}\right) \Gamma\left(\frac{3}{16}\right) \Gamma\left(\frac{5}{16}\right) \Gamma\left(\frac{7}{16}\right)} \approx 0.752, \quad (43)$$

$$|\Phi|_{\text{vertex}} = 2^{-1/4} \approx 0.841. \quad (44)$$

An expansion of the hypergeometric functions about the point at infinity can be avoided by a redefinition of the fundamental triangle, as explained in the caption to figure 2, thereby allowing the Higgs field at the vertex to be computed using (37) and (41), albeit with different values of the parameters.

Away from the points where the behaviour of the Higgs field can be studied analytically by known series expansions of the hypergeometric function, contours of $|\Phi|^2$ are obtained numerically and plotted using the auxiliary coordinate ζ as a parameter. This method leads to difficulty when sampling in the vicinity of the vertex of the octagon, since this is the image of the point at infinity in the ζ plane. A more effective procedure is to divide the octagon into eighths rather than sixteenths, so $(\alpha_1, \beta_1, \gamma_1) = (\frac{1}{4}, \frac{1}{8}, \frac{1}{8})$. The preimage of this triangle under $s_1(\zeta)$ is the entire upper half plane. Splitting the triangle into two further isosceles triangles as shown in figure 3, we find we need only sample within the region $|\zeta - 1| \leq 1$ (its complement in the upper half plane mapping to the other half triangle). After interpolating between gridpoints, the solution is analytically continued from \mathcal{O}_Δ to \mathcal{O} by Schwarz reflection, giving the contour plot of figure 4 (left).

Recall from section 3 that the octagon vertex and the origin are antipodal points on the Bolza surface. Placing a vortex at the origin breaks most of the symmetry of the Bolza surface, preserving a C_8 symmetry both at the vortex position and at its antipodal point. There should thus be a C_8 symmetry at the vertex of the octagon when a vortex is placed at the origin, but this is not easily seen. To see it more explicitly, let us shift the vortex to the vertex of the octagon. There should still be a C_8 symmetry at the origin. Recall that there is a double winding of f about the vortex position, which for the vortex at the origin maps from the $\{8, 8\}$ to the $\{4, 8\}$ tessellation. Angles measured at the vortex position are doubled as illustrated in figures 2 and 3. When the vortex is placed at a vertex, however, it is the angles at the vertices of \mathcal{O} which are doubled (from $\pi/4$ to $\pi/2$), while the map is conformal on the interior. The image is then an octagon in the $\{8, 4\}$ tessellation. The absence of ramification points on the interior of the octagon means the degree of the map is 1 and the Riemann-Hurwitz theorem tells us that the area of the image octagon is $A'_{\{8,4\}} = A_{\{8,8\}} - 2\pi = 2\pi$. Note that instead of (27), the more general formula for the area of the image polygon when N vortices are placed at the vertex is

$$A' = A - 2\pi N = 2\pi(2g - 2 - N), \quad (45)$$

which still implies the Bradlow bound (28). Dividing the domain and image polygons into triangles as before gives the contours of $|\Phi|^2$ shown in figure 4 (right).

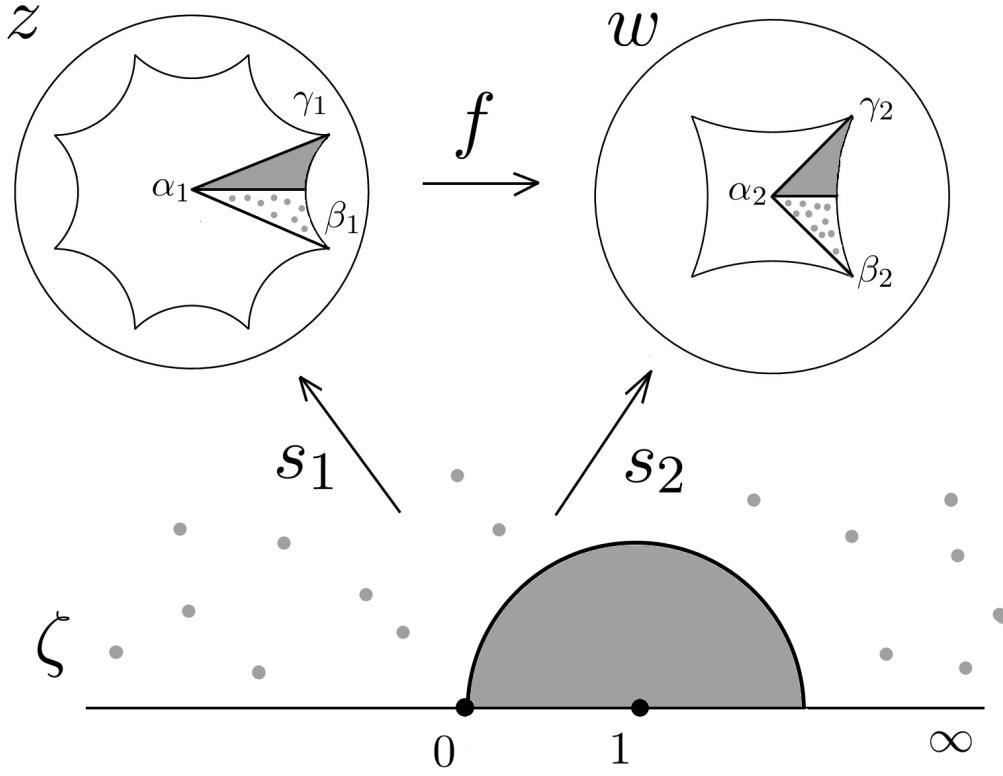


Figure 3: An alternative definition of the map f to that shown in figure 2. The resulting Higgs field is unchanged by this map. Shading indicates regions which map into each other, and the remainder of the hyperbolic plane is covered by reflections in the sides of the fundamental triangles. The advantage of this redefinition is improved numerical sampling (as the parameter ζ need only take values in a semi-disk), although it is harder to compute the value of $|\Phi|$ at the midpoint of an edge analytically as in (43). The angles of the triangles are $(\pi\alpha_1, \pi\beta_1, \pi\gamma_1) = (\frac{\pi}{4}, \frac{\pi}{8}, \frac{\pi}{8})$ and $(\pi\alpha_2, \pi\beta_2, \pi\gamma_2) = (\frac{\pi}{2}, \frac{\pi}{8}, \frac{\pi}{8})$.

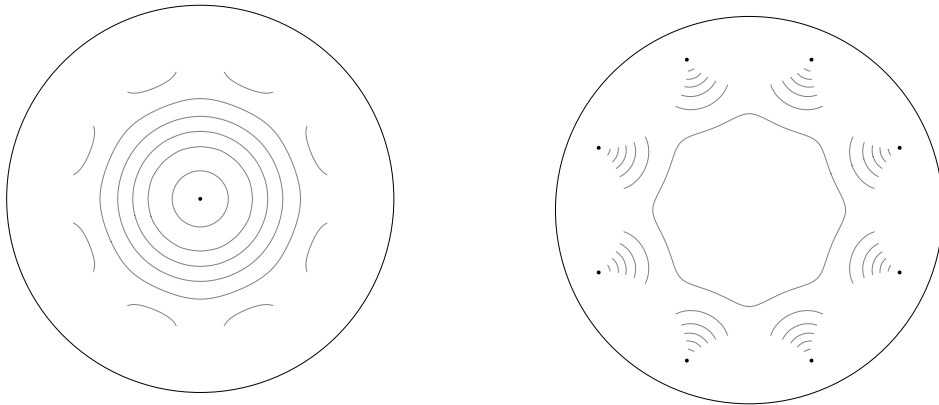


Figure 4: Contour plots of $|\Phi|^2$ for a vortex at the centre of the fundamental octagon (left) and at a vertex (right). $|\Phi|^2$ has a zero at the vortex position (marked by black dots) and reaches a maximum value of $1/\sqrt{2}$. The two configurations are equivalent due to the two preserved C_8 symmetries of the fundamental octagon (figure 1). The leading term of $|\Phi|^2$ near the centered vortex is at order $|z|^2$ and is circularly symmetric, while non-trivial angular dependence enters at order $|z|^{10}$.

4.4 Magnetic flux

We now proceed to check consistency of the magnetic flux. A single vortex has flux 2π , and we thus expect to obtain this value when B is integrated over the fundamental octagon. Using the same notation as in (4) the flux through the fundamental octagon \mathcal{O} can be computed using Stokes' theorem,²

$$\int_{\mathcal{O}} B \, dx dy = \int_{\partial\mathcal{O}} a_t dl = \int_{\partial\mathcal{O}} \left(\frac{1}{2} \partial_n h + \partial_t \chi \right) dl, \quad (46)$$

where dl denotes an infinitesimal line element of the boundary of the octagon, a_t is the tangential component of the gauge potential, and ∂_t and ∂_n are derivatives tangent to and normal to the boundary $\partial\mathcal{O}$. We note from figure 4 that the midpoints of the edges of the octagon are saddle points of $|\Phi|^2$. Combined with the reflection symmetry across the edges of the octagon we conclude that $\partial_n h$ vanishes everywhere on the boundary.

Let us now consider the topological contribution $\int_{\partial\mathcal{O}} \partial_t \chi \, dl$. On a segment of the boundary of \mathcal{O} , it evaluates to the difference in χ at the endpoints, $\Delta\chi$. From (8) we have, with $f' = \frac{df}{dz}$,

$$\chi = -\frac{i}{2} \log \left(f' \overline{f'}^{-1} \right). \quad (47)$$

²Recall from section 4.1 that $|\Phi|$ is invariant under transformations by the elements of the Fuchsian group H (20). It follows from the Bogomolny equations (2) that the physical magnetic flux density B/Ω is invariant under these transformations, although neither B nor Ω is invariant on its own. The physical magnetic flux is thus $\int (B/\Omega)(\Omega \, dx dy)$, where $\Omega \, dx dy$ is the area form on the Poincaré disk. Care must be taken to include the total derivative term $d\chi$ which affects the total flux, but does not alter the magnetic field locally.

Dividing the octagon into sixteenths as in figure 2, we carry out a rotation $z \mapsto ze^{i\pi/4}$ to take us from one vertex of the fundamental octagon to the next. From (25), this leads to $\chi \mapsto \chi + \pi/4$, hence the contribution to the flux from each edge of the octagon is $\pi/4$, and the total flux is 2π . Mapping between opposite edges of the fundamental octagon has the effect $\Delta\chi \mapsto \Delta\chi - \pi/2 = -\pi/4$, where the change in sign agrees with our traversing of the edge in the opposite direction.

It is interesting to compare our results with those for a single vortex placed at the origin of the Poincaré disk, \mathbb{H}^2 . From (12), this vortex has $f(z) = z^2$ and Higgs field (8)

$$|\Phi_0| = \frac{2|z|}{1 + |z|^2}. \quad (48)$$

Near the origin, $|\Phi_0| = 2|z| + \mathcal{O}(|z|^3)$, which should be compared to the result for the regular octagonal tessellation (42), where the leading coefficient of $|\Phi|$ at the vortex is approximately 1.768. To get a feel for the change in the fields near the origin when a single vortex on \mathbb{H}^2 is replaced by an $\{8, 8\}$ tessellation of vortices, we integrate the flux of the single vortex over the fundamental octagon of figure 1. As a fraction of the total flux, we find

$$\frac{1}{2\pi} \int_{\mathcal{O}} B_0 dx dy = \frac{8}{\pi} \sqrt{2\sqrt{2} - 2} \tan^{-1} \left(\sqrt{2\sqrt{2} + 2} \right) - 2 \approx 65.1\%, \quad (49)$$

showing that the lattice of vortices compresses the flux by about 50%.

5 Vortices on higher genus surfaces

The vortex equations on surfaces with $g > 2$ can be studied using similar arguments to those given in the preceding sections. The obvious extension of our construction is to a vortex at the origin of the Poincaré disk in the hyperbolic tessellation with Schläfli symbol $\{4g, 4g\}$. Quotienting by the Fuchsian group of the tessellation gives a vortex on a compact surface of genus g and area $4\pi(g-1)$. The fundamental $4g$ -gon is divided into $8g$ congruent triangles with angles $(\frac{\pi}{4g}, \frac{\pi}{2}, \frac{\pi}{4g})$. The map f is a two-to-one map from the $4g$ -gon to a $2g$ -gon in the $\{2g, 4g\}$ tessellation, and the image of the fundamental triangle is a triangle with angles $(\frac{\pi}{2g}, \frac{\pi}{2}, \frac{\pi}{4g})$. Applying the construction described in section 4.2 gives the maximum value of $|\Phi|$, measured at the vertex of the $4g$ -gon,

$$|\Phi|_{\max} = \frac{\Gamma\left(\frac{1}{4g}\right) \Gamma\left(\frac{3}{2g}\right)}{2 \Gamma\left(\frac{3}{4g}\right) \Gamma\left(\frac{1}{g}\right)} \sqrt{2 - \sec\left(\frac{\pi}{2g}\right)}, \quad (50)$$

and the coefficient of the leading term of $|\Phi|$ near the vortex at the origin,

$$|\Phi|_{\text{origin}} = \frac{\Gamma^3\left(\frac{1}{4g}\right) \Gamma\left(\frac{1}{2g}\right) \Gamma\left(\frac{3}{2g}\right)}{8\pi g \Gamma\left(\frac{3}{4g}\right) \Gamma^2\left(\frac{1}{g}\right)} \sqrt{\frac{\cot^2\left(\frac{\pi}{4g}\right) - 3}{\cot^2\left(\frac{\pi}{4g}\right) - 1}} |z| + \mathcal{O}(|z|^3). \quad (51)$$

As the genus is increased, the area available to a vortex grows linearly with g . The resulting increase in separation between adjacent vortices in the tessellation suggests that for large g , $|\Phi|$ should approach the solution $|\Phi_0|$ for a single vortex in \mathbb{H}^2 (48), which has $|\Phi_0|_{\max} = 1$ and $|\Phi_0|_{\text{vortex}} = 2|z| + \mathcal{O}(|z|^3)$. Evaluating (50) and the leading coefficient of (51) for some specific values of g , we do indeed approach this limit:

	$g = 2$	$g = 3$	$g = 4$	\cdots	$g \rightarrow \infty$
$ \Phi _{\max}$	0.841	0.965	0.986		1
$ z ^{-1} \Phi _{\text{origin}}$	1.768	1.955	1.984		2

The principal interest of higher genus surfaces is that the Bradlow bound (11, 28) allows them to hold more than one vortex. For example, for $g = 3$ the regular $\{12, 12\}$ tessellation with opposite edges identified allows one, two or three vortices placed at the origin or a vertex of the dodecagon. The Higgs field can again be computed by dividing the dodecagon into congruent triangles. Placing N_o vortices at the origin and N_v at the vertex of the dodecagon requires a map f with ramification of order $N_o + 1$ at the origin and $N_v + 1$ at the vertex. Thus the image tessellation is of type

$$\left\{ \frac{12}{N_o + 1}, \frac{12}{N_v + 1} \right\},$$

whose fundamental polygon has an area A' given by either (18) or the Riemann-Hurwitz theorem:

$$A' = 2\pi \frac{4 - N_o - N_v}{N_o + 1}. \quad (52)$$

The Bradlow bound requires that $N_o + N_v < 4$. This ensures that $N_o + 1$ and $N_v + 1$ both divide 12 and that the image tessellation is hyperbolic. The Euclidean tessellations of types $\{6, 3\}$ and $\{4, 4\}$ do not occur, because they would both require $N_o + N_v = 4$. It is easy to check using the expansion of the Schwarz triangle function (36) that $|\Phi|_{\text{origin}}$ behaves like $|z|^{N_o}$, with angular dependence at order $|z|^{N_o + 4g}$. Note that on more general $\{p, q\}$ tessellations, integer winding of f imposes divisibility constraints on N_o and N_v .

We remark that the surface described by the $\{12, 12\}$ tessellation with opposite edges identified is not the most symmetric genus 3 surface, which is the so-called Klein surface that can be represented by a $\{14, 7\}$ tessellation. However, our construction only allows us to place a single vortex on this surface, necessarily at the origin of the 14-gon (as $p \neq q$ the centres and vertices of the polygon are not equivalent). The image of the 14-gon is a heptagon in the $\{7, 7\}$ tessellation, and we obtain a vortex with C_7 symmetry with $|\Phi|_{\max} \approx 0.952$ and $|\Phi|_{\text{origin}} \approx 1.961|z| + \dots$

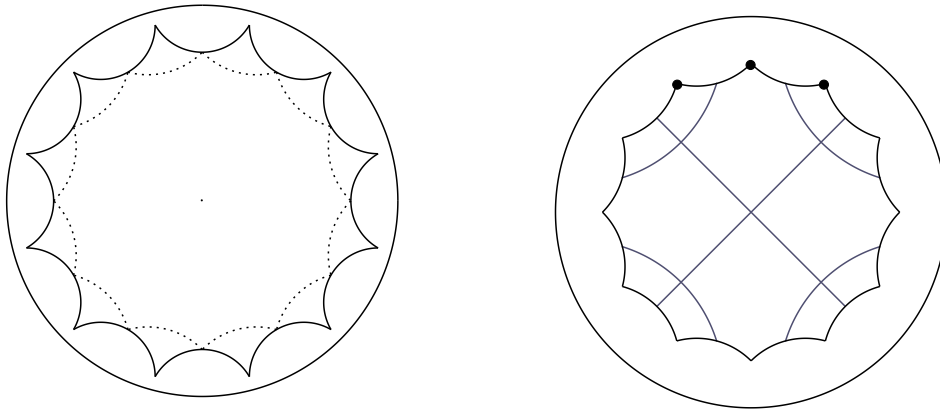


Figure 5: Left: the $\{12, 12\}$ tessellation with opposite edges identified (solid line) can be cut along the dotted line to give a dodecagon of half the area in the $\{12, 4\}$ tessellation. Identifying edges as shown in the right hand diagram yields a smooth compact genus 2 surface. Placing a vortex at the origin of the $\{12, 12\}$ cell and another at the vertex is therefore equivalent to a single vortex at the origin of a $\{12, 4\}$ cell. Three distinct vertices are indicated by dots.

5.1 A further quotient

A case of special interest is the $\{12, 12\}$ tessellation with one vortex placed at the origin of the dodecagon and one at the vertex. The image tessellation is of type $\{6, 6\}$. The leading behaviour of the Higgs field near each vortex is

$$|\Phi|_{\text{origin}} = \frac{2 - \sqrt{3}}{36\sqrt{2}} \frac{\Gamma^4(\frac{1}{12})}{\Gamma^4(\frac{1}{3})} |z| + \mathcal{O}(|z|^3) \approx 1.787|z| + \mathcal{O}(|z|^3). \quad (53)$$

We find the same leading coefficient when placing a single vortex at the origin of a dodecagon in the $\{12, 4\}$ tessellation. This result is due to the existence of a fixed-point-free \mathbb{Z}_2 action on the genus 3 surface which identifies the origin and vertex of the $\{12, 12\}$ tessellation. Quotienting by this group gives a smooth compact genus 2 surface with one vortex on it. This procedure is only possible when the vortex locations are compatible with the \mathbb{Z}_2 symmetry, and the quotient surface contains half the number of vortices. Figure 5 illustrates the relation between the two tessellations.

This observation can be understood by explicitly looking for a free \mathbb{Z}_2 action, an involution \mathcal{R} on the hyperelliptic curve. Let us generalise our discussion to a genus g surface represented by a regular $\{4g, 4g\}$ tessellation with opposite edges identified, with a vortex at the centre and another at the vertex. As a Riemann surface, this genus g surface is a double cover of \mathbb{CP}^1 with $2(g + 1)$ ramification points. The ramification points at the north and south poles correspond to the centre and vertex of the polygon, and there are $2g$ equally spaced ramification points on the equator. Generalising what was discussed in section 3 for the $g = 2$ Bolza surface, the cyclic C_{4g} symmetry has fixed points at the polygon centre and at the vertex, while there are g C_4 symmetries with

pairs of fixed points on the equator. The symmetry group of the surface is a double group of the dihedral group D_{2g} , and the hyperelliptic curve representing this setup is³

$$y^2 = x(x^{2g} + 1), \quad (x, y) \in (\mathbb{C}^*)^2. \quad (54)$$

The desired involution must map between the origin of the polygon and the vertex (i.e. between the poles of the sphere $x = 0$ and $x = \infty$) and have no fixed points. This is only possible for g odd (the case g even has fixed points at $(x, y) = (-1, \pm\sqrt{2}i)$), in which case it is achieved by the involution

$$\mathcal{R} : (x, y) \mapsto (x^{-1}, -yx^{-g-1}). \quad (55)$$

The quotient of the branched cover of \mathbb{CP}^1 by this involution is a double covering of the northern hemisphere with a particular identification of the segments of the equator between ramification points. In the polygon picture, there are $4g$ edges to pair up. Consistency with the transformation $x \mapsto x^{-1}$ gives two possible pairings for each edge, due to the choice of branch. We also require the quotient surface to be smooth, which will be the case if there is no angle deficit at the identified vertices. The total internal angle of the quotient $\{4g, 4\}$ polygon is $2\pi g$, hence there must be g distinct vertices when the edges are paired. This imposes a further constraint on our choice of edge identifications. There is also the possibility that edge pairs can be twisted, although it is not clear whether our construction, which relies on $f(z)$ extending from a fundamental triangle to all of \mathbb{H}^2 by reflections, works in the twisted case. Once the correct identifications have been made, the resulting surface has half the area of the original surface and genus $\frac{1}{2}(g + 1)$.

The identification described in the preceding paragraphs is illustrated for the $g = 3$ case in figure 5. The genus 2 surface in the $\{12, 4\}$ tessellation has different Fenchel-Nielsen parameters from the $\{8, 8\}$ tessellation, and they therefore represent different surfaces. An immediate consequence of this is the different leading behaviour of the Higgs field, as is seen by contrasting (42) and (53). Because a 2-holed surface has no freely acting rotations by π , the genus cannot be reduced further.

6 Conclusions and outlook

In this paper we have shown how to construct Abelian-Higgs vortices on compact hyperbolic surfaces which can be represented by tessellations of the hyperbolic plane by regular polygons. Placing vortices on the surface breaks most of the symmetry, and our method requires the vortex positions to be chosen in such a way that there is a preserved symmetry allowing the surface to be covered by congruent triangles sharing vertices at the vortex positions. In particular, multivortex solutions can be constructed with vortices located at antipodal points on the surface, corresponding to the origin and vertex of the polygonal tessellation. The Higgs field is computed by identifying a holomorphic

³In the special case of the Bolza surface ($g = 2$), the symmetry is enhanced to $GL(2, 3)$, a double cover of the cubic group.

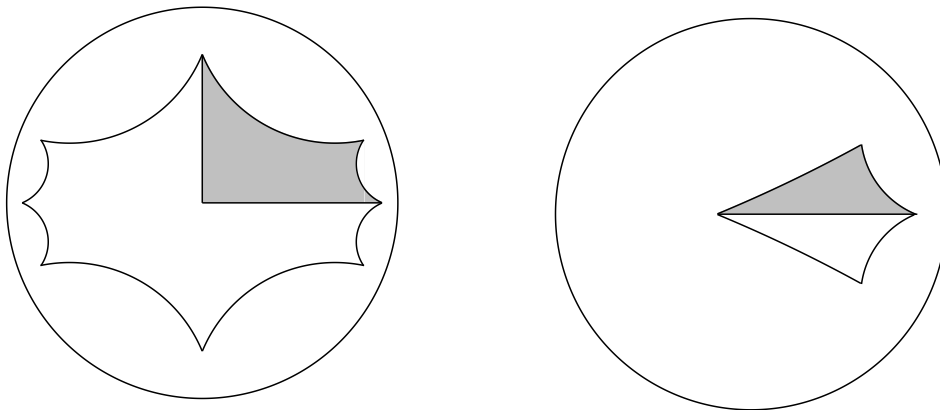


Figure 6: An example of a deformed $\{8, 8\}$ octagon with angles of $\pi/4$ which can be split into four quadrilaterals, each of which maps to half of a deformed image quadrilateral.

function on the fundamental polygon which is conformal everywhere except at the vortex positions, where there is a ramification point of order one greater than the number of vortices at that location. This function can be expressed implicitly as the composition of two Schwarz triangle functions, allowing numerical evaluation of the Higgs field at any given point on the surface.

There are several immediate generalisations of this procedure which it would be interesting to investigate further:

- The tessellation can be deformed such that the angles are fixed but the edge lengths change (see figure 6). In this case we require a map from a quadrant of the fundamental octagon to half a kite. The construction is analogous to that of the Schwarz triangle map described in section 4, with the hypergeometric differential equation (30) replaced by the Heun differential equation, which has four regular singular points. The difficulty with this construction is the appearance of an *accessory parameter* which characterises the deformation, and which requires numerical computation. A different deformation of the regular octagon was studied in [7].
- The construction described in this paper does not allow the vortex to be placed at an arbitrary position on the surface. The Riemann map from a hyperbolic polygon to the upper half plane is analytically continued to cover the Poincaré disk by reflection in the edges of the polygon. If the vortex is not positioned symmetrically then the fields cannot be constructed by maps between regular polygons. As it stands, our construction only enables us to compute the fields at isolated points in the moduli space.
- A final outstanding question is how to place an arbitrary number N of vortices (with $N < 2g - 2$) at the origin of a symmetric tessellation describing a genus g surface. An $(N + 1)$ -fold map from the fundamental polygon to a smaller polygon

is only possible if $N + 1$ divides the number of edges of the initial polygon. For example, we can place a single vortex on the Klein surface (with a map from a 14-gon to a heptagon), but not two or three vortices.

Acknowledgements

This work was supported by the UK Science and Technology Facilities Council under grant number ST/J000434/1.

References

- [1] A. Jaffe, C. Taubes, *Vortices and Monopoles*, Birkhäuser (1980)
- [2] J. M. Baptista, *Vortices as degenerate metrics*, Lett. Math. Phys. **104** (2014) 731, [arXiv:1212.3561 \[hep-th\]](#)
- [3] E. Witten, *Some exact multipseudoparticle solutions of classical Yang-Mills theory*, Phys. Rev. Lett. **38** (1977) 121
- [4] U. Essmann, H. Träuble, *The direct observation of individual flux lines in type II superconductors*, Phys. Lett. **A 24** (1967) 526
- [5] N. S. Manton, N. A. Rink, *Vortices on hyperbolic surfaces*, J. Phys. A **43** (2010) 434024, [arXiv:0912.2058 \[hep-th\]](#)
- [6] W. J. Floyd, S. P. Plotnick, *Growth functions on Fuchsian groups and the Euler characteristic*, Invent. Math. **88** (1987) 1
- [7] A. V. Nazarenko, *Two-parametric hyperbolic octagons and reduced Teichmüller space in genus two*, [arXiv:1301.5446 \[math-ph\]](#)
- [8] Z. Nehari, *Conformal Mapping*, McGraw-Hill (1952)
- [9] M. Harmer, G. Martin, *Conformal mappings from the upper half plane to fundamental domains on the hyperbolic plane*, Department of Maths Report Series 499, University of Auckland, N.Z. (2003)